On the two types of steady hard X-ray states of GRS 1915+105.

Sergey P. Trudolyubov[1,2]

ABSTRACT

Using the data of 5 years of *RXTE* observations we investigate the X-ray spectral and timing properties of GRS 1915+105 during the *hard steady* states. The broad-band energy spectrum of the source during these periods is dominated by extended hard component with characteristic cut-off/ break at $\sim 10-120$ keV. The power density spectrum of the source rapid aperiodic variability shows dominant band-limited white noise component breaking at few Hz accompanied by a group of strong QPO peaks and in some cases an additional high frequency noise component with characteristic cut-off at $\sim 60-80$ Hz.

According to the results of our simultaneous X-ray spectral and timing analysis the behavior of the source during the *hard steady* states can be reduced to a couple of major distinct types. i) *Type I states:* The dominant hard component of the energy spectrum has characteristic quasi-exponential cut-off at $50-120$ keV. The broad-band power density spectrum of the source shows significant high frequency noise component with a cut-off at $\sim 60-80$ Hz. ii) *Type II states:* The hard spectral component has a break in its slope at $\sim 12-20$ keV. The high frequency part of the power density spectrum fades quickly lacking significant variability at frequencies higher than ~ 30 Hz. These two types of the X-ray hard states are also clearly distinguished by their properties in the radio band: while during the *type I* observations the source tends to be 'radio-quiet', the *type II* observations are characterized by high level of radio flux (*'plateau'* radio states).

In this work we demonstrate aforementioned differences using the data of 12 representative *hard steady* state observations. We conclude that the difference between these two types can be probably explained in terms of different structure of the accretion flow in the immediate vicinity of the compact object due to presence of relativistic outflow of matter.

[1]NIS-2, Los Alamos National Laboratory, Los Alamos, NM 87545; tsp@nis.lanl.gov

[2]Space Research Institute, Russian Academy of Sciences, Profsoyuznaya 84/32, Moscow, 117810 Russia

1. INTRODUCTION

The X-ray source GRS 1915+105, the first Galactic object found to generate superluminal jets (Mirabel & Rodriguez 1994), was discovered by the *GRANAT* observatory as a transient in 1992 (Castro-Tirado, Brandt & Lund 1992). Long-term monitoring of GRS 1915+105 with the *RXTE* satellite (Bradt et al. 1993) has revealed a rich character of the source transient activity associated with different levels of its luminosity, which can be reduced to the sequence of varying *soft steady*, *flaring* and *hard steady* states qualitatively distinguished by their spectral and temporal properties (Greiner et al. 1996; Trudolyubov et al. 1999*a*; Muno et al. 1999). It was demonstrated that the major spectral and temporal properties of the source during these periods are similar to that of the Galactic black hole candidates in the 'canonical' spectral states (Chen et al. 1997; Taam et al. 1997; Trudolyubov et al. 1999*a*).

For almost a half of the observational time the source demonstrates steady periods characterized by a relatively hard broad–band X-ray spectrum and X-ray luminosity $\sim (1-6) \times 10^{38} ergs/s$ (assuming the source distance of 12.5 kpc) – *hard steady* states (Muno et al. 1999; Belloni et al. 2000). In general, the energy spectrum of GRS 1915+105 during these periods can be approximated by a sum of the weak soft thermal component with characteristic color temperature $\sim$ 1 keV and dominant extended hard component with turnover at high energies (Fig. 1) (Trudolyubov et al. 1999*a*; Muno et al. 1999). The variation of the X-ray flux on the time scale of an individual observation does not exceed $\sim 20\%$. The power density spectrum (PDS) of the source is dominated by strong band-limited white noise (BLN) component accompanied by system of QPO peaks with centroid frequencies of several Hz (Fig. 2) (Morgan et al. 1997; Chen et al. 1997; Trudolyubov et al. 1999*a*). The pattern of correlation between X-ray and radio emission of the source is complicated: alternating periods of high (so-called 'plateau states') and low level radio emission associated with hard steady states have been reported (Foster et al. 1996; Fender et al. 1999; Muno et al. 1999).

In this work we demonstrate that the source shows two distinct branches of the *hard steady* state (hereafter *type I* and *type II*), distinguished by the properties of its energy spectrum, high frequency X-ray variability and level of radio flux. We discuss the difference between these two types of the *hard steady* states in the framework of the two-phase model of the inner part of accretion flow, involving the outflow from the immediate vicinity of the compact object.

2. OBSERVATIONS AND RESULTS

The *RXTE* satellite performed regular pointed observations of GRS 1915+105 in 1996 – 2000 providing a good coverage for the detailed study of the spectral and timing properties of the source in the *hard steady* states. In the Table 1 we listed the groups of observations covering *hard steady* states and individual representative observations used for the detailed analysis.

2.1. Spectral and timing analysis

For the processing of the PCA and HEXTE data we used standard *RXTE* FTOOLS (version 5.01) tasks and methods recommended by *RXTE* Guest observer Facility.

For spectral analysis, we used PCA *Standard 2* mode data, collected in the $3-20$ keV energy range. The PCA response matrices for individual observations were constructed using PCARMF v7.01, and background estimation was performed applying a Very-Large Events (VLE)–based model. Standard dead time correction procedure has been applied to the PCA data. Owing to the uncertainties of the response matrix, a 1% systematic error was added to the statistical error for each PCA energy channel. We used the HEXTE response matrices, released on October 20, 1998 and subtracted background collected in off-source observations for each cluster of detectors. In order to account for the uncertainties in the response and background determination, only data in the $20-150$ keV energy range were used for the spectral analysis. Typical examples of the broad-band energy spectra of GRS 1915+105 during the *hard steady* states in 1996 – 2000 are shown in Fig. 1.

As we are interested in the general properties of the source energy spectrum during the *hard steady state*, we used only simple models to approximate its spectra. For the first group of observations showing a hard spectra with clear cut-off at the energies $\sim 60-90$ keV (Fig. 1, *panels a, b, c*), we used only HEXTE data in the $20-150$ keV energy range and approximated them by power law with exponential cut-off (Table 2, *first part*). For the remaining observations (Fig. 1, *panels d, e, f*) data of PCA and HEXTE instruments covering the $3-150$ keV energy range were approximated by absorbed broken power law (Table 2, *second part*). For all cases there was a distinct residuals corresponding to the iron emission /absorption, thus Gaussian line profile and an absorption edge were included to refine the overall fit. An equivalent hydrogen absorbing column density was fixed at the level of $N_H L = 5 \times 10^{22}$ cm^{-2}.

For the timing analysis in the $2-30$ keV energy range the *RXTE*/PCA data in the *binned* and *event* modes containing X-ray events below and above 13 keV respectively

were used. We generated power density spectra (PDS) in the $0.001 - 512$ Hz frequency range combining the results of the summed Fourier transforms of a short stretches of data (8 s) with 0.001 s time bins for the $0.3 - 512$ Hz frequency range, and a single Fourier transform on the data in 0.125 s time bins for lower frequencies. The resulting spectra were logarithmically rebinned, when necessary, to reduce scatter at high frequencies, and normalized to square root of fractional variability *rms*. The white noise due to the Poissonian statistics corrected for the dead time effects, was subtracted (Zhang et al. 1995; Revnivtsev et al. 2000). Typical examples of the broad-band power density spectra of GRS 1915+105 during *hard steady* state (in units of $f \times (rms/mean)^2$ (Belloni et al. 1997)) are shown in Fig. 2.

Broad-band power density spectrum (PDS) of the source is dominated by a strong band-limited white noise (BLN) component with at least two characteristic breaks (at ~ 0.1 and ∼few Hz) and a complex of relatively narrow peaks of quasi-periodic oscillations (QPO) lying near the second break in the slope of BLN continuum (Fig. 2). For some observations (Fig. 2, *panels a, b, c*), the additional broad high frequency component with characteristic cut-off at $\sim 60 - 80$ Hz was also notable.

To quantify the properties of the source rapid aperiodic variability, PDS in the $0.05 - 256$ Hz frequency range were fitted to analytic models using χ^2 minimization technique. We used a combination of two BLN components (approximated by zero-centered Lorentzian functions) and several QPO features (presented by the Lorentzian functions). For some observations (Fig. 2, *panels a, b, c*), an additional high frequency noise component was approximated by zero-centered Gaussian function with characteristic width of $\sim 60 - 80$ Hz. Parameters of the PDS approximation are presented in Table 3.

2.2. Two types of X-ray hard steady states

As it is seen from Figs. 1 and 2, representative *hard steady* state observations can be subdivided into two distinct classes with qualitatively different spectra and PDS. Further we will refer to these groups of observations as *type I* and *type II* states (see Table 2,3). Below we summarize characteristic spectral and timing properties of both groups.

Type I states. The energy spectrum is dominated by an extended power law hard component with photon index $\alpha \sim 1.8 - 2.3$ and quasi- exponential cut-off at $\sim 60 - 90$ keV (Fig. 1(*panel a, b, c*); Table 2). Broad-band PDS shows prominent noise component with average integrated *rms* amplitude of $\sim 4 - 5\%$ and characteristic cut-off frequency of $\sim 60 - 80$ Hz, detectable up to ~ 150 Hz (Fig. 2, *panel a, b, c*; Table 3). An average total

fractional *rms* amplitude of the rapid aperiodic variability in the $2-30$ keV energy range is about $\sim 22\%$ (Table 3).

Type II states. The energy spectrum exhibits clear break in power law slope near $\sim 13-16$ keV. High energy part of the spectrum has roughly power law shape with almost constant photon index of $\alpha \sim 3.2-3.3$, in spite of significant changes in the slope of the lower energy part (Fig. 1, *panel d, e, f*; Table 2). As in case of *type I* states, the PDS of the source is dominated by BLN and QPO components with characteristic peaks at a few Hz. Contrary to the *type I* states, high frequency part of the PDS in the *type II* state fades quickly lacking any significant variability above ~ 30 Hz. For some observations an additional noise component with characteristic cut-off at ~ 15 Hz was marginally detected (Table 3). The average total fractional *rms* amplitude of the rapid aperiodic variability in the $2-30$ keV energy range is $\sim 5\%$ lower than during the *type I* state observations (Table 3).

2.3. Correlated properties of X-ray and radio emission

To trace the simultaneous evolution of GRS 1915+105 in radio band we used publicly available data of the Green Bank Interferometer monitoring observations at 8.3 GHz (Foster et al. 1996). Fig. 3 shows examples of the X-ray and radio lightcurves of the GRS 1915+105 during the *hard steady* state in $1997-1998$. We note that all periods of *type I* X-ray *hard steady* state correspond to low level of radio emission (the flux at 8.3 GHz is typically lower than $10-20$ mJy). [3] On the other hand, periods of *type II* state are characterized by much higher level of radio flux ($\sim 50-100$ mJy). *Type II* state is also referred as a quasi-stable *'plateau'* radio state with flat radio spectrum (Foster et al. 1996; Fender et al. 1999) and accompanying bright infrared emission (Bandyopadhyay et al. 1998). To explain the properties of the source during *'plateau'* states the formation of the optically thick radio source powered by outflow of matter from the system was proposed (Fender et al. 1999).

3. DISCUSSION

To explain the observational properties of black hole binaries in the *hard* and *very high* states (Tanaka & Lewin 1995) a number of models involving the hot Comptonization

[3]Note, that the short 'spikes' seen on the radio lightcurve correspond to the X-ray *flaring* states, occasionally interrupting *hard steady* states

region near the compact object surrounded by the optically thick accretion disk (Shakura & Sunyaev 1973) were proposed (Chakrabarti & Titarchuk 1995). According to these models the soft thermal component of the energy spectrum is emitted by the optically thick accretion disk, while the hot inner region is responsible for generation of the hard spectral component. It was proposed that low and high frequency noise components in the power density spectrum are associated with outer optically thick and inner optically thin parts of the accretion flow respectively (Miyamoto et al 1994). It is often assumed that QPO phenomenon is caused by the interaction between these two distinct parts of the accretion flow occurring on the local dynamical time scale at the boundary between these regions related to the local Keplerian time (Molteni et al 1996; Titarchuk, Lapidus & Muslimov 1998). Supporting this model, the evidence of the correlation between an observed QPO frequency and the position of the boundary between optically thick and optically thin parts of the accretion flow was reported for the *flaring* states of GRS 1915+105 (Trudolyubov et al. 1999*b*; Chakrabarti & Manickam 2000).

It looks natural to suggest that band limited white noise dominating the PDS of GRS 1915+105 may also be a product of the dynamic processes in the inner part of the accretion flow. Then the dynamic time scales on both inner and outer boundaries of this region will determine an extent of the resulting noise spectrum in the frequency domain. Given the position of high frequency cut-off in the PDS and radial dependence of the dynamic oscillation frequency, one can estimate an approximate position of the inner boundary of the optically thin region. Let us discuss individual properties of the two branches of the *hard steady* state on the basis of the above assumptions. We assume that characteristic frequencies of the QPO and BLN noise components of the power density spectra of the GRS 1915+105 are proportional to the Keplerian frequency at the outer and inner boundaries of the optically thin region of accretion flow, i.e. $f = f_K/l$, where $f_K \approx 2200\, m^{-1} r^{-3/2}$ Hz, m – mass of the compact object in solar masses, r – distance to the compact object in units of 3 gravitational radii.

Type I state: If the hard spectral component originates through the Comptonization of the low energy photons in the optically thin inner region, the observed cut-off energy of the spectrum indicates high electron temperature in this part of the accretion flow, $kT_e \sim 20 - 40$ keV (Sunyaev & Titarchuk 1980). Typical value of the QPO centroid frequency allows one to estimate an approximate position of the outer boundary of the optically thin part of the accretion flow: $r_{out} \sim 170(m f_{QPO} l)^{-2/3}$. Broad high-frequency component detected in all *type I* state observations is of particular interest. The position of the characteristic break of this component $f_{cut}^{high} \sim 60 - 80$ Hz (Table 3) is remarkably close to the position of the reccurent stable QPO at 67 Hz observed mainly during the *soft steady* state (Morgan et al. 1997; Remillard & Morgan 1998). This fact provides a possibility that

the broad noise component can be related to this steady QPO and be interpreted as the effective broadening of the coherent oscillation feature. Most of the models explaining the stable 67 Hz QPO invoke some kind of oscillations near the inner edge of the accretion disk in the immediate vicinity of the compact object (Morgan et al. 1997 and references therein). These oscillations may explain the high-frequency noise component detected during the *type I* state observations.

Type II state: The properties of the X-ray and radio emission of GRS 1915+105 in *type II* state imply significantly different geometry and characteristics of the accretion flow compared to that of *type I* state. We suggest two possible interpretations of the observed shape of the hard spectral component in the *type II* state. Thermal Comptonization mechanism implies relatively low electron temperature in the inner region, $kT_e \sim 5$ keV. On the other hand, the observed break in the hard component can be explained as due to the transmission of the hard X-rays through dense surrounding matter with average Thomson optical depth of the order of several (assuming power law shape of the spectrum of illuminating radiation) (Sunyaev & Titarchuk 1980). Typical value of the QPO centroid frequency during the *type II* states is close to that of the *type I* states, indicating possible similarity in the position of the outer boundary of the optically thin part of the accretion flow. As it is seen from Fig. 2, the PDS of the *type II* state demonstrates the lack of significant variability of the source at frequencies above ~ 30 Hz. This fact may hint at the larger inner radius of the hot comptonization region with respect to the *type I* state. Assuming noise generation mechanism described above, and given the characteristic cut-off frequencies of the PDS in the *type I* ($f_I^{high} \sim 70$ Hz) and *type II* ($f_{II}^{high} \sim 15$ Hz) state (Table 3), the ratio of the inner radii of the accretion flow, r_I^{in} and r_{II}^{in} can be estimated as $(r_{II}^{in}/r_I^{in}) \sim (f_I^{high}/f_{II}^{high})^{2/3} \sim 3$. To explain higher value of the inner radius in the *type II* state, the effective mechanism of the truncation of the accretion flow near the compact object in this state is needed. The observations at the radio and infrared wavelengths indicate the presence of a strong outflow of matter near the compact object coupled with a hot inner region (Fender et al. 1999; Eikenberry et al. 1998). It is usually assumed that such outflows originate very close to the compact object, modifying the structure of the innermost part of the accretion flow. Finally, we may suppose that contrary to the *type I* state in the *type II* state the accretion flow extends down to some transition radius, followed by outflow region in the immediate vicinity of the compact object.

As a result, the difference between the properties of X-ray and radio emission of GRS 1915+105 during *type I* and *type II hard steady* states may be explained in terms of the different structure of the inner part of the accretion flow. Contrary to the *type I* X-ray state, in the *type II* state an inner region of the accretion flow coupled with a strong outflow of matter near the compact object, which causes the aforementioned differences in the

observational properties.

Finally, our two types of the *hard steady* states may be compared with the previous systems of 'states' used to characterize X-ray variability of GRS 1915+105. According to the definition, the 'C' state of Belloni et al. (2000) (with four classes of variability χ_1, χ_2, χ_3, χ_4) corresponds to our *hard steady* state. It should be also noted that similar distinction for a limited sample of $1996-1997$ 'hard steady' observations based on the level of radio flux was proposed by Muno et al. (1999). The 'radio-loud hard steady state' and 'radio-quiet hard steady state' of Muno et al. (1999) are directly associated with our *type I* and *type II hard steady* states.

This research has made use of data obtained through the High Energy Astrophysics Science Archive Research Center Online Service, provided by the NASA/Goddard Space Flight Center. The Green Bank Interferometer is a facility of the National Science Foundation operated by the NRAO in support of NASA High Energy Astrophysics programs.

REFERENCES

Bandyopadhyay, R., Martini, P., Gerard, E., Charles, P. A., Wagner, R. M., Shrader, C., Shahbaz, T., Mirabel, I. F. 1998, MNRAS, 295, 623

Belloni, T., van der Klis, M., Lewin, W. H. G., van Paradijs, J., Dotani, T., Mitsuda, K., & Miyamoto, S. 1997, A&A, 322, 857

Belloni, T., Klein-Wolt, M., Mendez, M., van der Klis, M., & van Paradijs, J. 2000, A&A, 355, 271

Bradt, H., Swank, J., & Rothschild, R. 1993, A&AS, 97, 355

Castro-Tirado, A., Brandt, S. & Lund, N. 1992, IAU Circ. 5590

Chakrabarti, S. K., & Titarchuk, L. G. 1995, ApJ, 452, 226

Chakrabarti, S. K., & Manickam, S. G. 2000, ApJ, 531, L41

Chen, X., Swank, J. H., & Taam, R. E. 1997, ApJ, 477, 723

Eikenberry, S. S., Matthews, K., Murphy, T. W., Nelson, R. W., Morgan, E. H., Remillard, R. A., & Muno, M. 1998, ApJ, 506, L31

Fender, R. P., Garrington, S. T., McKay, D. J., Muxlow, T. W. B., Pooley, G. G., Spencer, R. E., Stirling, A. M., & Waltman, E. B. 1999, MNRAS, 304, 865

Foster, R. S., Waltman, E. B., Tavani, M., Harmon, B. A., Zhang, S. N., Paciesas, W. S., Ghigo, F. D. 1996, ApJ, 467, L81

Greiner, J., Morgan, E. H., & Remillard, R. A. 1996, ApJ, 473, L103

Mirabel, I., F., & Rodriguez, L. F. 1994, Nature, 371, 46

Miyamoto, S., Kitamoto, S., Iga, S., Hayashida, K., & Terada, K. 1994, ApJ, 435, 398

Molteni, D., Sponholz, H., & Chakrabarti, S. K. 1996, ApJ, 457, 805

Morgan, E. H., Remillard, R. A., & Greiner, J. 1997, ApJ, 482, 993

Muno, M. P., Morgan, E. H., & Remillard, R. A. 1999, ApJ, 527, 321

Rao, A. R., Naik, S., Vadawale, S. V., & Chakrabarti, S. K. 2000, A&A, 360, L25

Reig, P., Belloni, T., van der Klis, M., Mendez, M., Kylafis, N. D., Ford, E. C. 2000, ApJ, 541, 883

Remillard, R. A., & Morgan, E. H. 1998, preprint (astro-ph/9805237)

Revnivtsev, M., Gilfanov, M., & Churazov, E. 2000, A&A, 363, 1013

Shakura, N. I., & Sunyaev, R. A. 1973, A&A, 24, 337

Sunyaev, R. A., & Titarchuk, L. G. 1980, A&A, 86, 121

Taam, R., Chen, X., & Swank, J. H. 1997, ApJ, 485, L83

Tanaka, Y., & Lewin, W. H. G. 1995, in X-ray Binaries, ed. W. H. G. Lewin, J. Van Paradijs, & E. P. J. van den Heuvel (Cambridge: Cambridge Univ. Press), 126

Titarchuk L., Lapidus I., & Muslimov, A. 1998, ApJ, 499, 315

Trudolyubov, S., Churazov, E., & Gilfanov, M. 1999*a*, Astron. Lett., 25, 718

Trudolyubov, S., Churazov, E., & Gilfanov, M. 1999*b*, A&A, 351, L15

Zhang, W., Jahoda, K., Swank, J. H., Morgan, E. H., & Giles, A. B., 1995, ApJ, 449, 930

Table 1: The list of *RXTE* observations of GRS 1915+105 in the *hard steady* states. The information on the individual representative observations is shown in column 3 (Obs. ID/Date, UT).

RXTE Proposal ID	Dates, UT	Obs. ID/Date, UT	Ref.
10258, 10408	Jul. 23, 1996 – Sep. 03, 1996	10258-01-01-00/Jul. 23, 1996	1, 2, 4, 6
		10258-01-04-00/Aug. 14, 1996	
10408, 20402	Oct. 23, 1996 – Apr. 25, 1997	20402-01-07-00/Dec. 19, 1996	3, 4, 5, 6
		20402-01-15-00/Feb. 09, 1997	
20187, 20402	Oct. 05, 1997 – Oct. 25, 1997	20402-01-49-00/Oct. 08, 1997	5, 6
		20402-01-51-00/Oct. 22, 1997	
30402, 30703	Apr. 04, 1998 – Jul. 27, 1998	30703-01-14-00/Apr. 06, 1998	7
		30703-01-20-00/May 24, 1998	
30402, 30703	Aug. 28, 1998 – Oct. 10, 1998	30402-01-17-00/Sep. 11, 1998	7
		30703-01-35-00/Sep. 25, 1998	
30703, 40703	Dec. 26, 1998 – Mar. 27, 1999	40703-01-01-00/Jan. 01, 1999	7
	Jun. 02, 1999 – Jun. 07, 1999		8
	Dec. 01, 1999 – Feb. 21, 2000		7
50405, 50703	Mar. 08, 2000 – May. 05, 2000	50405-01-03-00/Apr. 23, 2000	7

1 – Chen et al. 1997

2 – Morgan et al. 1997

3 – Trudolyubov et al. 1999*a*

4 – Muno et al. 1999

5 – Reig et al. 2000

6 – Belloni et al. 2000

7 – this work

8 – Rao et al. 2000

Table 2: Spectral parameters of GRS 1915+105 in the *hard steady* state. Parameter errors correspond to 1σ confidence level.

Type I[a]					
Date (UT)	Power Law Index	Cut-Off energy (keV)	χ^2 (d.o.f.)	Flux[b]	
19/12/1996	2.22 ± 0.06	85 ± 15	130.0(115)	2.141	
09/02/1997	1.83 ± 0.05	63 ± 5	185.5(154)	1.521	
11/09/1998	2.20 ± 0.17	66 ± 11	35.6(37)	2.274	
25/09/1998	2.04 ± 0.07	66 ± 7	75.8(76)	2.018	
01/01/1999	2.17 ± 0.06	66 ± 8	176.2(154)	2.215	
23/04/2000	2.23 ± 0.08	83 ± 14	78.7(76)	1.985	
Type II[c]					
Date (UT)	Power Law Index	Break Energy (keV)	Power Law Index	χ^2 (d.o.f.)	Flux[b]
23/07/1996	2.37 ± 0.01	14.0 ± 0.3	3.29 ± 0.01	237.3(193)	2.640
14/08/1996	2.75 ± 0.01	13.5 ± 0.5	3.33 ± 0.02	274.4(233)	2.487
08/10/1997	2.76 ± 0.01	15.9 ± 0.5	3.31 ± 0.02	161.8(116)	2.273
22/10/1997	2.48 ± 0.01	16.1 ± 0.1	3.21 ± 0.01	382.7(233)	2.053
06/04/1998	2.54 ± 0.01	13.1 ± 0.3	3.33 ± 0.02	274.8(153)	2.434
24/05/1998	2.38 ± 0.01	15.9 ± 0.1	3.23 ± 0.02	130.7(116)	2.190

[a] – HEXTE data, $20 - 150$ keV energy range, power law model with exponential cut-off

[b] – total energy flux in the $3 - 150$ keV energy range in units of $\times 10^{-8}$ erg s^{-1} cm^{-2}

[c] – PCA and HEXTE data, $3 - 150$ keV energy range, absorbed broken power law model

Table 3: The characteristics of the power density spectra of GRS 1915+105 during the *type I* and *type II hard steady* states. rms_{tot}, rms_{QPO} and rms_{high} represent total *rms* amplitude, *rms* amplitude of the fundamental QPO harmonic and *rms* amplitude of the additional high frequency noise component integrated over the $0.05 - 512$ Hz frequency range. f_{QPO} and f_{high}^{cut} denote the centroid frequency of the fundamental QPO peak and characteristic break frequency of the high frequency component. Parameter errors correspond to a 1σ confidence level.

Date (UT)	rms_{tot} (%)	f_{QPO} (Hz)	rms_{QPO} (%)	f_{high}^{cut} (Hz)	rms_{high} (%)
			Type I		
19/12/1996	22.31 ± 0.05	3.13 ± 0.01	12.10 ± 0.14	63 ± 4	4.42 ± 0.32
09/02/1997	24.61 ± 0.07	2.25 ± 0.01	12.60 ± 0.19	69 ± 3	5.39 ± 0.32
11/09/1998	19.66 ± 0.06	3.67 ± 0.01	11.22 ± 0.14	79 ± 9	3.53 ± 0.44
25/09/1998	24.84 ± 0.08	2.45 ± 0.01	12.86 ± 0.23	62 ± 7	4.86 ± 0.43
01/01/1999	25.82 ± 0.05	2.27 ± 0.01	15.10 ± 0.18	63 ± 4	4.30 ± 0.25
23/04/2000	24.25 ± 0.08	2.88 ± 0.01	12.83 ± 0.20	80 ± 9	4.15 ± 0.51
			Type II		
23/07/1996	16.30 ± 0.10	0.49 ± 0.01	11.12 ± 0.21	...	...
14/08/1996	15.73 ± 0.04	2.68 ± 0.01	8.79 ± 0.19	16 ± 2	2.14 ± 0.63
08/10/1997	13.81 ± 0.05	$2.62 - 2.96$	10.71 ± 0.20	...	...
22/10/1997	18.16 ± 0.05	1.39 ± 0.01	11.45 ± 0.18	15 ± 2	2.85 ± 0.72
06/04/1998	16.11 ± 0.08	$1.53 - 1.69$	12.15 ± 0.31	...	...
24/05/1998	16.07 ± 0.09	0.70 ± 0.01	10.02 ± 0.25	...	...

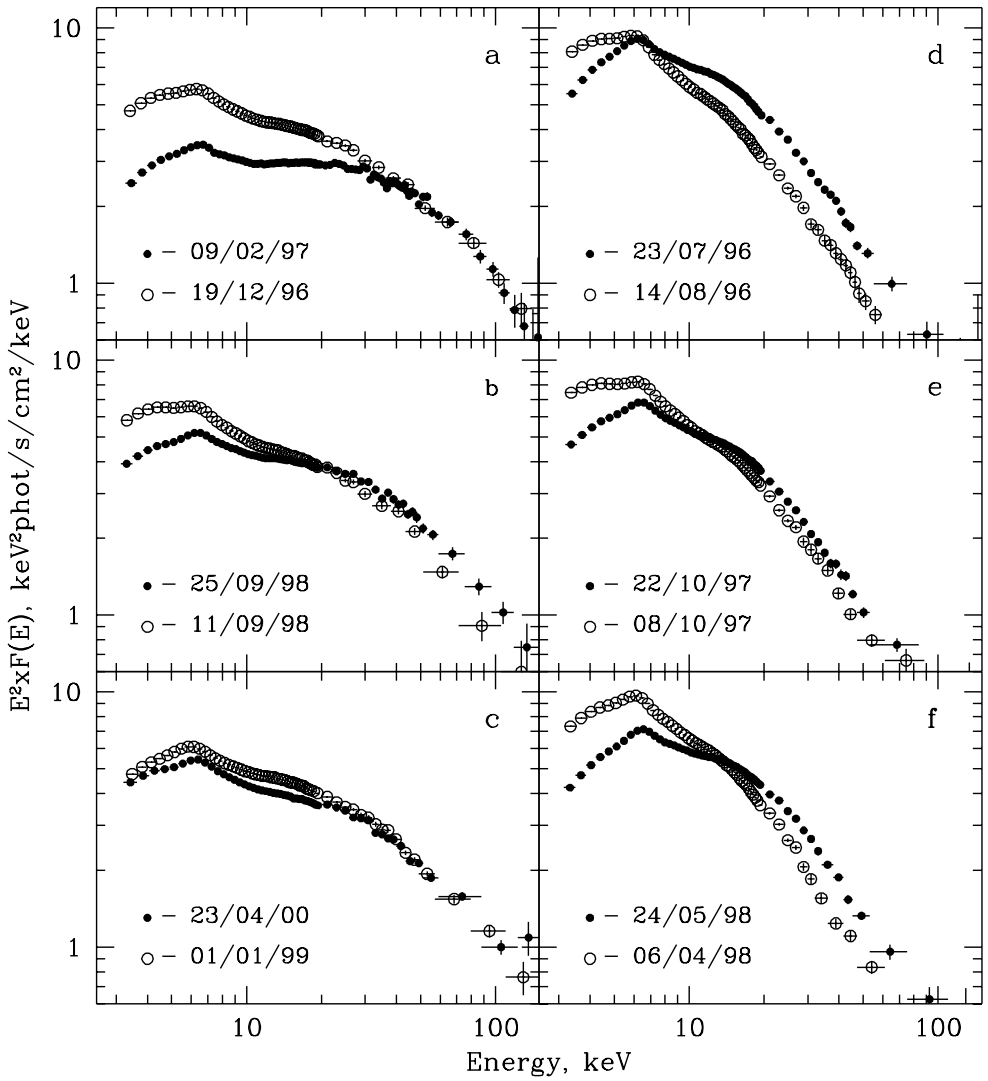

Fig. 1.— Broad-band energy spectra of GRS 1915+105 (in units of $E^2 \times F(E)$) corresponding to the *type I* (*panels a, b, c*) and the *type II* (*panels d, e, f*) *hard steady* states.

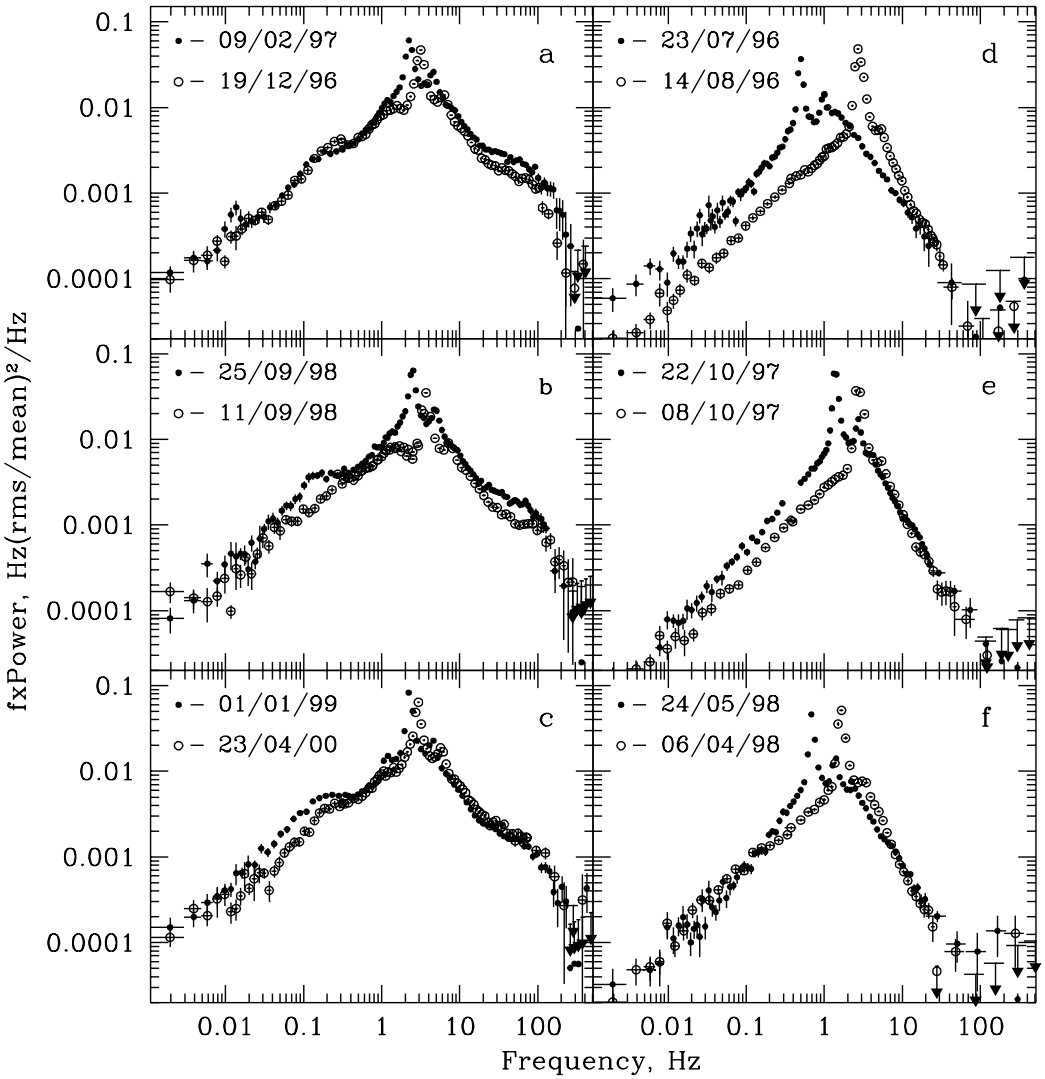

Fig. 2.— Power density spectra (PDS) of GRS 1915+105 (in units of $f \times P(f)$) corresponding to the *type I* (*panels a, b, c*) and the *type II* (*panels d, e, f*) *hard steady* states. Note the prominent high-frequency band-limited white noise component in the *type I* PDS.

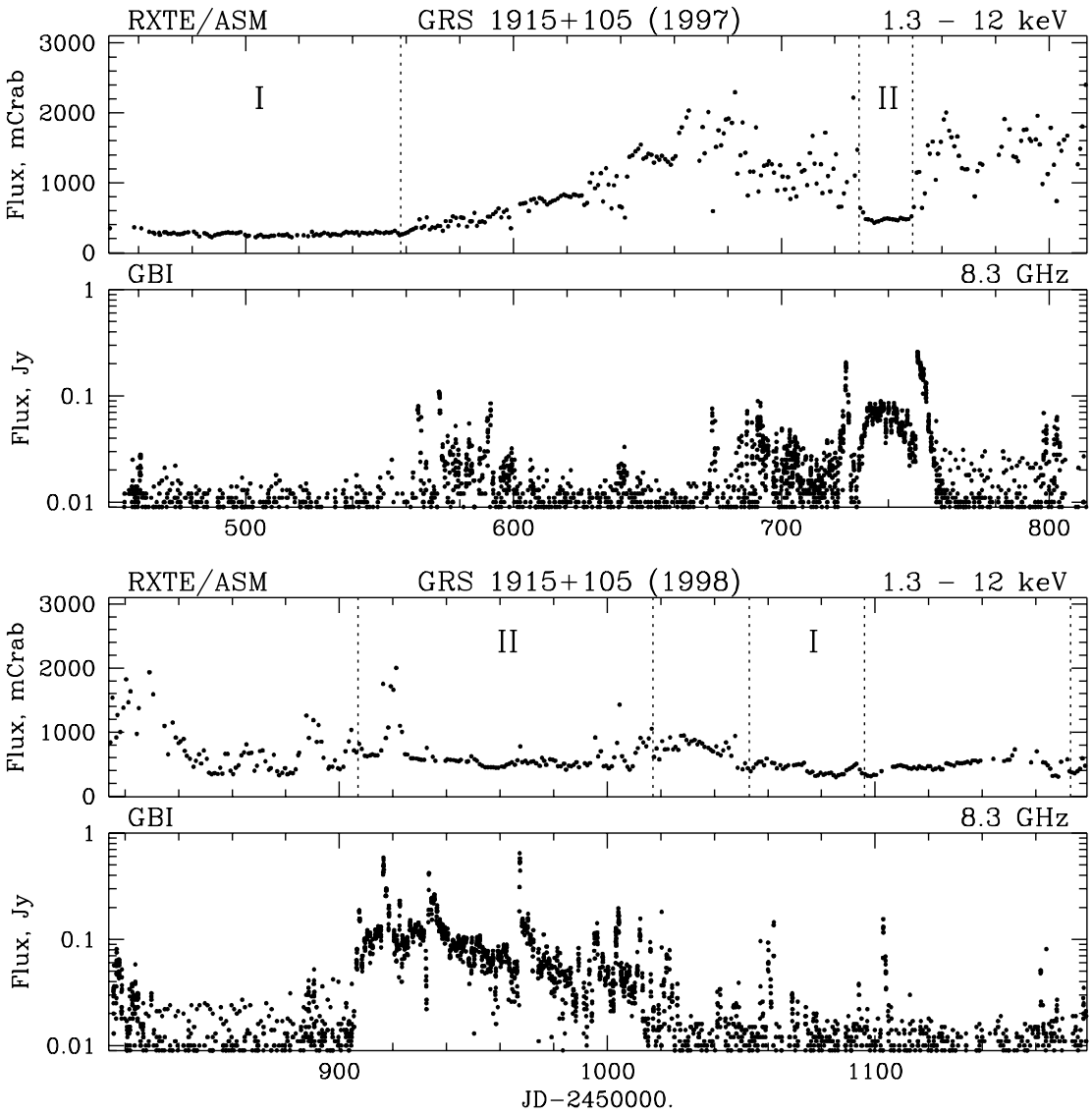

Fig. 3.— Simultaneous X-ray and radio lightcurves of GRS 1915+105 in 1997 and 1998. The boundaries of the *type I* and *type II hard steady* states are marked by dotted lines. The X-ray flux is in the mCrab units (1 mCrab $\sim$ 0.075 cnts s^{-1}) (*RXTE*/ASM and Green Bank Interferometer (GBI) data)